Semnan University

Progress in Physics of Applied Materials

journal homepage: https://ppam.semnan.ac.ir/

Hydrothermal Synthesis of Chitosan Nitrogen-Doped Graphene for Supercapacitors Applications

Fatemeh Khojasteh [a], Salimeh Kimiagar [b*]

[a] *Department of Physics, Central Tehran Branch, Islamic Azad University, 14696-69191, Ayatollah Hashemi Complex in Poonak, Tehran, Iran*

[b] *Nanophysics Research Lab (NRL), Department of Physics, Central Tehran Branch, Islamic Azad University, 14696-69191, Ayatollah Hashemi Complex in Poonak, Tehran, Iran*

ARTICLE INFO

Article history:
Received: 11 January 2025
Revised: 1 February 2025
Accepted: 2 February 2025

Keywords:
Supercapacitor;
Chitosan Nitrogen-doped Graphene;
Reversibility;
Cyclic Voltammetry;
Charge-discharge.

ABSTRACT

In this paper, a chitosan nitrogen-doped graphene (CNGO) electrode is synthesized by using carbon paper (CP). This electrode demonstrates enhanced electrochemical properties as a supercapacitor electrode compared to CP. The CNGO nanocomposite is synthesized using a hydrothermal method and is deposited on CP via dip coating method. To characterize the CNGO nanocomposite, X-ray diffractometer (XRD), Fourier transform infrared spectroscopy (FTIR), field emission scanning electron microscopy (FESEM), and energy dispersive spectroscopy (EDS) mapping analyses are performed. The electrochemical properties of the electrodes are studied through cyclic voltammetry, galvanostatic charge-discharge (GCD), and electrochemical impedance spectroscopy. The specific capacitance is increased from 29.73 $\frac{mF}{cm^2}$ for the CP to 43.6 $\frac{mF}{cm^2}$ for the CNGO electrodes at a current density of $2\frac{mA}{cm^2}$. The reversibility ratio is calculated to be 0.89 and 0.94 for CP and CNGO electrodes, respectively. The proposed electrode demonstrates exceptional performance due to its outstanding stability and durability over extended cycling, as evidenced by its 100% capacitance retention after 1100 charge-discharge cycles. This remarkable retention highlights its ability to maintain consistent electrochemical properties under prolonged and repetitive operational conditions. The results indicate that the presence of CNGO nanocomposite on CP enhances the electrochemical properties of the electrode.

1. Introduction

The increasing global demand for efficient, reliable, and sustainable energy storage solutions has driven substantial progress in green energy technologies. As concerns regarding climate change, energy security, and environmental degradation grow, the transition toward renewable energy sources has become imperative. Green energy sources, such as solar, wind, and hydroelectric power, are increasingly recognized as pivotal to reducing global dependence on fossil fuels, thereby mitigating their detrimental environmental impacts. However, the intermittent nature of renewable energy necessitates the development of advanced energy storage systems that can efficiently store and deliver energy as required.

Supercapacitors have emerged as one of the most promising energy storage technologies, classified under electrochemical capacitors. They play a crucial role in complementing or even replacing traditional energy storage devices, such as batteries, in various applications. Unlike conventional batteries, supercapacitors utilize electrochemical transformations to store energy, offering a cleaner, greener, and more sustainable alternative for energy storage and delivery [1]. Their unique properties, including high power density, rapid charge and discharge cycles, and extended cycle life, position them as an attractive solution for applications requiring fast energy bursts and

* Corresponding author. Tel.: +98-912-1230921
E-mail address: s_kimiagar@iauctb.ac.ir

Cite this article as:
Khojasteh F. and Kimiagar S., 2025. Hydrothermal Synthesis of Chitosan Nitrogen-Doped Graphene for Supercapacitors Applications. *Progress in Physics of Applied Materials*,5(1), pp.85-95. DOI: **10.22075/PPAM.2025.36551.1128**

long operational reliability [2]. These attributes make supercapacitors ideal for use in electric vehicles, grid stabilization, and portable electronic devices, among other applications. Supercapacitors effectively bridge the performance gap between traditional capacitors and batteries. Traditional capacitors are known for their exceptional power density but suffer from limited energy density, while batteries offer high energy density but are constrained by lower power density and shorter cycle life. Supercapacitors combine the strengths of both technologies, enhancing the performance of energy storage systems by improving power output and durability, which leads to greater system reliability and efficiency [3]. This unique capability allows them to augment battery performance, extend battery life, and provide backup power during peak demand periods.

Research and development efforts in supercapacitor technology have largely focused on enhancing key performance parameters, such as energy density, power density, and operational stability [4]. A primary area of innovation lies in the development of advanced electrode materials, which play a vital role in determining the overall performance of supercapacitors. Materials such as metal oxides, carbon-based nanomaterials, and conductive polymers have demonstrated significant potential in enhancing the energy storage capacity and efficiency of supercapacitors.

Recent studies have showcased remarkable advancements in electrode material fabrication and optimization. Nawwar et al. (2019) developed carbon nanotubes decorated with magnetite particles, achieving a capacitance of 5.82 F/cm^2 in a 0.5 M sodium sulfate (Na_2SO_4) electrolyte [5]. Similarly, Polat et al. (2024) synthesized $ZnFeO_4$ on nickel foam with a high graphene content, leading to a notable increase in electrode performance and a specific capacitance of 622 mF/cm^2 [6]. Zhang et al. (2024) improved supercapacitor energy density by incorporating spherical nanocarbon clusters within a green, ionic electrolyte, reporting a specific capacitance of 0.091 F/m^2 [7]. These advancements underscore the importance of electrode material design in achieving superior energy storage capabilities. One of the most effective strategies for enhancing energy density involves the development of doped carbon electrode materials that offer a high specific surface area. This approach increases the number of active sites available for ion adsorption and redox reactions, thereby improving overall capacitance and energy storage capacity [8]. Kishore et al. (2024) fabricated sponge-like porous carbon from biomass, which provided a fine porous structure ideal for doping with heteroatoms such as nitrogen and sulfur. This doping process resulted in improved specific capacitance and enhanced cyclic stability [9].

Building on these advancements, the present study aims to synthesize a novel nanocomposite of chitosan and nitrogen-doped graphene oxide (NGO) for supercapacitor electrode fabrication. Chitosan, a biodegradable and environmentally friendly polymer, offers excellent film-forming ability and mechanical strength, while NGO contributes high electrical conductivity and enhanced electrochemical performance. The nanocomposite is deposited onto a carbon paper (CP) electrode to improve its efficiency and overall performance. This enhanced electrode holds significant potential as an effective solution for green energy storage applications, aligning with the global push toward sustainable energy technologies.

2. Experiment Details

2.1. Materials

Urea, sodium monohydrogen phosphate, sodium dihydrogen phosphate, and acetic acid were all purchased from Merck KGaA. Ethanol (99.8%) was supplied by Qazvin Chemical Company, while sodium hydroxide was procured from SISCO Research Laboratories PVT. LTD, India. Nano graphene oxide powder was sourced from Nano Materials at Tarbiat Modares University, Iran. Chitosan was acquired from the Shiraz Science and Technology Park in Iran. Carbon paper was obtained from JNTG Company in South Korea.

2.2. Synthesis Method

First, 0.25 g of graphene oxide and 7.5 g of urea were combined in 100 mL of ethanol in a beaker and stirred with a magnetic stirrer for 1 h. The mixture was then transferred to a sealed stainless steel autoclave reactor and heated in an oven at 180°C for 12 h to synthesize NGO. After cooling to room temperature, the product was washed with deionized water and ethanol through centrifugation at 6000 RPM for 15 minutes. Finally, the product was dried on a watch glass at room temperature.

Next, 0.5g of chitosan was mixed with 100 mL of deionized water containing 1% acetic acid and stirred for 8 h. Separately, 1g of the NGO was mixed with 0.5g of ammonia in 100 mL of deionized water and stirred for 8 h. The two mixtures were then combined and further stirred for an additional 8 h. The resulting mixture was washed twice with deionized water and ethanol by centrifugation at 6000 RPM for 15 minutes, and then dried at 120°C for 5 h. To deposit the resulting nanocomposite onto CP, the powder was first mixed with deionized water and deposited on CP by dip-coating method. The coated CP was then dried at 120°C for 5 h.

2.3. Electrochemical Experiments

Cyclic voltammetry is a technique that applies a varying voltage to an electrode while measuring the resulting current. This method provides insights into the electrode's charge storage capacity and the speed at which it can release stored charge. A buffer solution and three electrodes were utilized for the analysis: the fabricated sample, a silver/silver chloride (Ag/AgCl) electrode, and a platinum electrode. The voltage was swept between the fabricated sample and the Ag/AgCl reference electrode within a range of $\Delta V = 2V$, spanning from -1V to 1V. The current response was recorded.

3. Experiment Details

3.1. Characterization

The structural properties of the samples were analyzed by a Philips Xpert- MPD Model 3040 X-ray diffractometer (XRD) with Cu Kα radiation with λ=1.5406 Å. In Fig. 1a the peak at 2θ = 28° is assigned to the (002) plane of NGO, confirming the reduction of GO through the restoration of van der Waals interactions between the carbon frameworks on the graphene sheets during the reduction process [10, 11]. Fig 1b shows chitosan peaks at 2θ = 18.2, 20.1, 29.2, 31.8, 33.9, 47.1, and 50.8 [12-14]. In the XRD pattern of the CNGO nanocomposite, peaks from both chitosan and NGO are present, which appear with a slight shift, indicating strain within the nanocomposite (Fig. 1c).

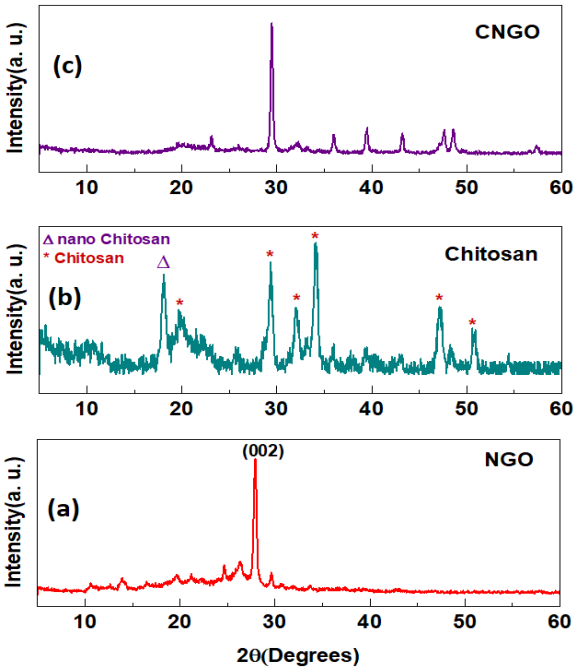

Fig. 1. XRD pattern of the (a) NGO, (b) chitosan, and (c) CNGO

Fourier transform infrared spectroscopy (FTIR) was obtained within the range of 600-4000 cm^{-1} (Thermo, AVATAR, US). In Fig. 2a the characteristic peaks for NGO are: a broad peak around 3700 cm^{-1} (O–H stretching vibrations) indicating the presence of hydroxyl groups [15]. This peak indicates the presence of non-hydrogen-bonded hydroxyl groups on the surface of the material. A peak near 1720 cm^{-1} (C=O stretching vibrations) is associated with carbonyl groups [16]. A peak around 1620 cm^{-1} (C=C stretching vibrations) corresponds to the sp^2 hybridized carbon framework of graphene [16]. Peaks in the range of 1200–1350 cm^{-1} (C–N stretching vibrations) indicate the C–N bonds resulting from nitrogen doping [16]. These peaks confirm the incorporation of nitrogen atoms into the graphene lattice and the presence of various oxygen-containing functional groups.

Chitosan peaks in Fig. 2b: a broad peak around 3450 cm^{-1} (O–H and N–H stretching vibrations) indicating the presence of hydroxyl and amine groups. Peaks near 2920 cm^{-1} and 2880 cm^{-1} (C–H stretching vibrations) corresponding to aliphatic C–H bonds. A peak around 1650 cm^{-1}, amide I band (C=O Stretching), associated with the carbonyl group in the amide linkage. A peak around 1066 cm^{-1} (C–O–C stretching vibrations) is indicative of the glycosidic linkage in chitosan [17, 18]. The FTIR spectrum of CNGO exhibits characteristic peaks from both chitosan and NGO (Fig. 2c). The peak at 3440 cm^{-1} for chitosan has shifted to 3435 cm^{-1} and broadened, attributed to the overlapping O–H and NH_3^+ stretching bands. The peak at 1730 cm^{-1} corresponds to the stretching vibrations of the carbonyl group (C=O). The amide I band, observed at 1650 cm^{-1}, represents the C=O stretching vibrations of chitosan. A peak at 1575 cm^{-1} is associated with C=C stretching, indicating the presence of aromatic rings in graphene. Amide III bands, occurring between 1300–1400 cm^{-1}, correspond to N–H bending and C–N stretching of chitosan. The peak at 1150 cm^{-1} is attributed to C–O–C stretching, while the peaks between 600–1000 cm^{-1}, representing C–H bending, serve as the fingerprint region for carbohydrates [19, 20].

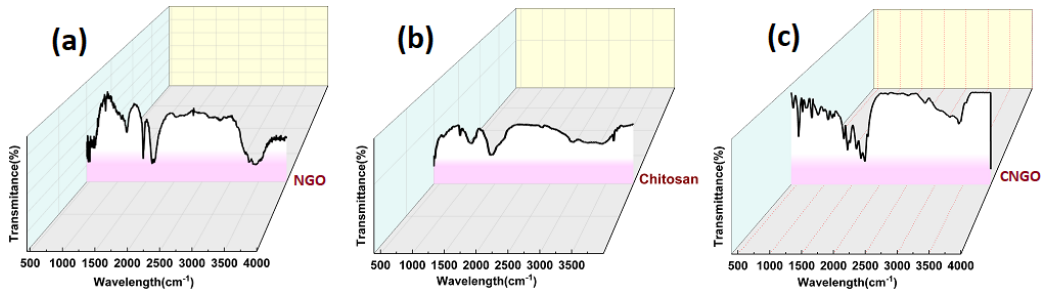

Fig. 2. FTIR of the (a) NGO, (b) chitosan, and (c) CNGO

The morphology was analyzed using a field emission scanning electron microscope (FESEM) (MIRA III model, TESCAN). Fig. 3a shows the FESEM image of the CNGO nanocomposite, while Fig. 3b displays that of the deposited nanocomposite on CP. The presence of the nanocomposite between the CP fibers increases the surface area-to-volume ratio of the electrode, allowing electrons to move more freely. This enhancement improves the current and electrochemical properties of the electrode, which will be discussed in detail later. Energy-dispersive X-ray spectroscopy (EDS) was conducted to identify the chemical elements in the synthesized CNGO nanocomposite (TESCAN, VEGA 3 model with a French SAMX detector, Czech Republic). The EDS image shows the distribution of different elements in the electrode, which is crucial for analyzing the chemical composition.

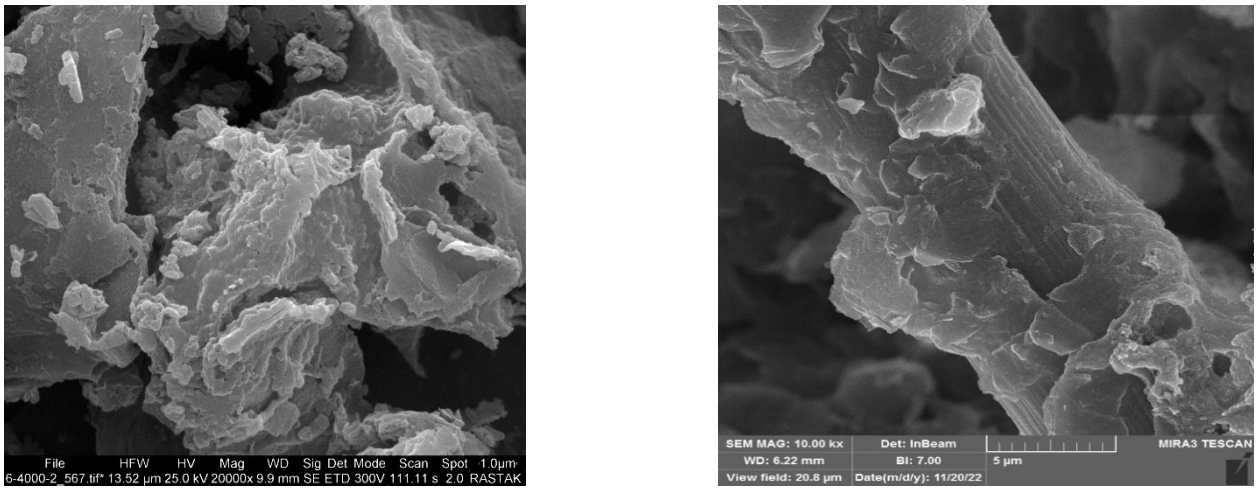

Fig. 3. FESEM images of (a) CNGO nanocomposite and (b) CNGO nanocomposite on CP

Energy-dispersive X-ray spectroscopy (EDS) was conducted to identify the chemical elements in the synthesized CNGO nanocomposite (TESCAN, VEGA 3 model with a French SAMX detector, Czech Republic). The EDS image shows the distribution of different elements in the electrode, which is crucial for analyzing the chemical composition. Fig. 4 confirms the presence of N, C, and O in the sample, indicating that the CP contains the nanocomposite (Fig. 4a-c). The composition of all materials in the electrode is shown in Fig. 4d.

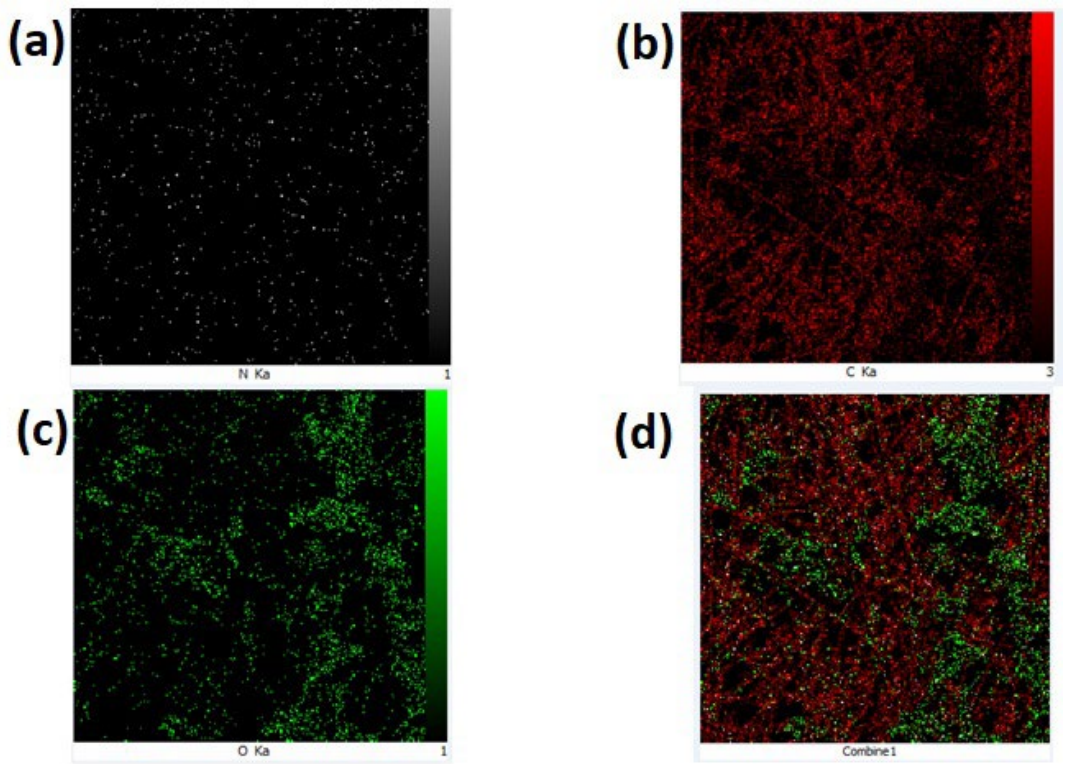

Fig. 4. X-Map of the CNGO nanocomposite

To measure the specific surface area of the nanocomposite, BET (Brunauer-Emmett-Teller, BEL Company, BELSORP MINI II, Japan)) analysis with N_2 as the carrier gas was performed at a constant temperature of 0°C. The gas adsorption temperature on the material's surface was set at -196°C (the temperature of liquid nitrogen) to minimize effects such as gas evaporation or

pressure fluctuations. The results are presented in Table 1. The specific surface area of the CNGO nanocomposite has increased compared to that of chitosan. The increase in surface area results in more active sites on the electrode surface for ion adsorption and desorption [21, 22]. The increase in surface area and mean pore diameter in the nanocomposite leads to an increase in energy density in the supercapacitor electrode, making it more efficient for energy storage applications [23].

Table 1. The calculated data from BET analysis

Sample	Mass (g)	Specific surface area ($m^2.g^{-1}$)	Mean pore diameter(nm)
CNGO	0.1045	9.5891	22.429
Chitosan	0.1650	7.8977	0.918

3.2. Electrochemical Measurements

An Autolab potentiostat/galvanostat 302N was used to study the current intensity response to variations in potential difference. A three-electrode system in an electrochemical cell, consisting of a working electrode with a surface area of 1 cm^2, a platinum electrode to reduce solution resistance and ensure current transport by diffusion, and a silver/silver chloride (Ag/AgCl) reference electrode, was employed. A buffer solution of Na_2HPO_4 and NaH_2PO_4 with a pH of 7.4 was used as the electrolyte, which is environmentally friendly and widely utilized in the water treatment industry.

In Fig. 5a and 5b, the cyclic voltammetry of CP and CNGO electrodes at scan rates (SR) of 70, 110, 170, and 220 mV/s is compared. The cyclic voltammetry behavior indicates that the three-electrode system operates as an asymmetric supercapacitor [24]. This result was expected because the materials of the working and reference electrodes are different. In an asymmetric or hybrid supercapacitor, the behavior of electric double-layer capacitors and quasi-capacitor supercapacitors coexist. In quasi-capacitor supercapacitors, chemical changes occur due to the redox process (oxidation and reduction). The quasi-capacitive behavior of the CNGO electrode is evident from the presence of sharp oxidation and reduction peaks.

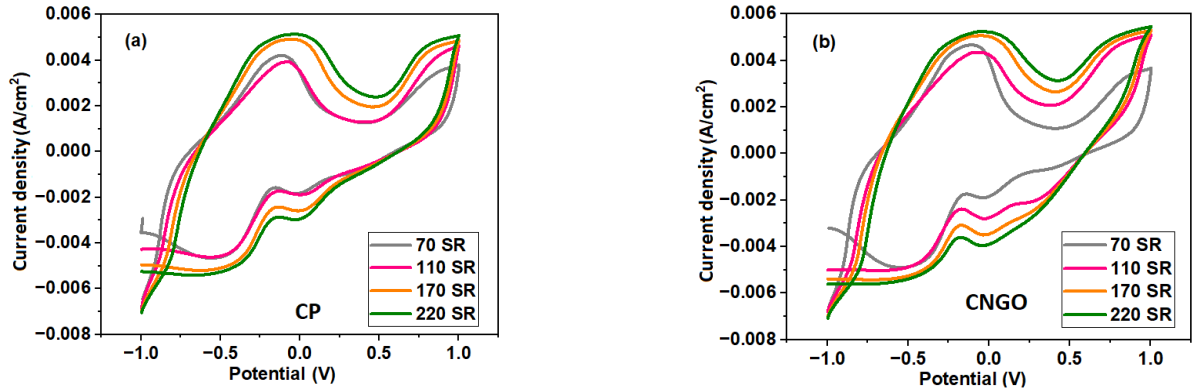

Fig. 5. Cyclic voltammetry of (a) CP and (b) CNGO electrodes

To calculate the capacitive capacity, the cyclic voltammetry technique is used. This method is one of the widely employed techniques in electrochemistry, aiding in the analysis of the electrochemical behavior of materials during charge and discharge processes. The equation 1 calculates the specific capacitance of the electrode material [25-27]:

$$C = \frac{\int I\, dv}{v\, A\, \Delta V} = \frac{\int I_A dv}{v\, \Delta V} \qquad (1)$$

where the stored charge during the cyclic voltammetry process (the integral of current versus potential over a cycle) is divided by the scan rate (mV/s), the electrode surface area A (cm^{-2}), and the potential window(ΔV). The area under the cyclic voltammetry curve represents the variations in current as a function of potential differences during the process.

A comparison of the results in Fig. 6 shows that the specific capacitance of the CNGO electrode is higher than that of the CP electrode at the corresponding scan rate. Therefore, the presence of the nanocomposite in the CNGO electrode has improved the performance of the electrochemical supercapacitor electrode.

Two conventions are generally used to report CV data: the US and IUPAC conventions. Visually data reported in the two conventions will appear to be rotated by 180^0 [28].

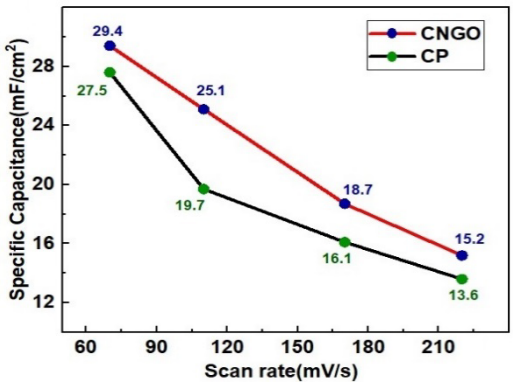

Fig. 6. Specific capacitance of CP and CNGO electrodes

In carbon-based materials, an anodic peak in the forward reaction and two cathodic peaks in the reverse

process are often observed in electrochemical measurements such as cyclic voltammetry. The anodic peak arises due to the oxidation of functional groups on the carbon surface or quinone groups or from faradaic redox reactions. In the reverse scan, two distinct cathodic peaks may appear, corresponding to different reduction processes. The first cathodic peak typically results from the reduction of oxidized functional groups, while the second peak may be attributed to processes like oxygen reduction, electrolyte ion adsorption, or additional faradaic reactions [29]. In Fig. 7a and 7b, one anodic peak in the forward reaction and two cathodic peaks in the reverse process are observed. The main reduction reaction in an electrochemical system is crucial because it determines the fundamental redox process governing the system's behavior. However, identifying the primary reduction reaction can be challenging due to overlapping signals from side reactions, surface interactions, or electrolyte effects. Reversibility is generally determined based on the primary reaction associated with the anodic and cathodic peaks. Intermediate reactions often arise from indirect chemical interactions, such as the formation of complexes or unstable species that are rapidly reconverted into the original reactants or products. These reactions are usually treated as independent of the main reaction since they respond differently to changes in voltage sweep rate and are not necessarily linked to the number of electrons exchanged in the primary reaction [30]. Phosphate buffer is primarily used to maintain the system's pH and conductivity, with a low likelihood of direct electrochemical reactions involving phosphate ions [30].

The Anodic peak is labeled as (AP) and the Cathodic peak is marked as (CP). From equation 2, the reversibility ratio of this reaction can be estimated by considering the kinetics of electron transfer and a scan rate of 70 mV/s, as follows [31]:

$$\left|\frac{I_{AP}}{I_{CP}}\right| \cong 1 \tag{2}$$

In equation 2, the closer this ratio is to 1, the greater the reversibility of the electrode. The values of ΔE and $\left|\frac{I_{AP}}{I_{CP-2}}\right|$ for the redox peak of the CP and the CNGO electrode are presented in Table 2. The smaller absolute value of ΔE in the CNGO electrode indicates improved stability and more controlled electrochemical reactions in the cell. The ratio of the anodic peak to the cathodic peak in the CNGO electrode is closer to 1, indicating better electrode efficiency and improved energy storage [32].

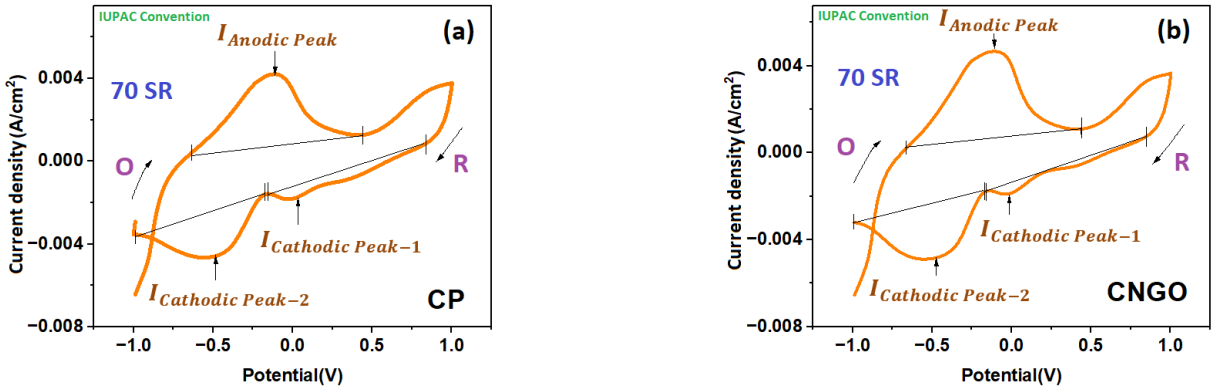

Fig. 7. Anodic and cathodic peaks of (a) CP and (b) CNGO electrodes for 70 mV/s scan rate

Table 2. Reversibility ratio and ΔE calculation in the main redox peak of cyclic voltammetry (Fig. 5)

Electrode	$\Delta E = E_{CP-2} - E_{AP}(V)$	$I_{AP}(mA)$	$I_{CP-2}(mA)$	$\left\|\frac{I_{AP}}{I_{CP-2}}\right\|$
CP	-0.473	4.16	-4.66	0.89
CNGO	-0.443	4.61	-4.89	0.94

The GCD method is used to study the performance of CP and CNGO electrodes (Fig. 8a and 8b). The selected current density rates were 2, 7, and 15 mA/cm^2 for both the CP and CNGO electrodes. A comparison of the results shows that, with increasing current density, the charging and discharging times decrease [33]. As current density increases, a greater electric charge crosses the electrode surface per unit of time. Increasing current density reduces the time required to charge, implying that less energy is stored within this time frame. Similarly, in the discharging the stored energy is released more rapidly. As observed, the charging and discharging times for the CNGO electrode are longer than those for the CP electrode at various current densities. The presence of nanocomposite between the carbon paper fibers increases the contact surface area, enhancing the likelihood of electrochemical reactions.

The specific capacitance from Fig. 8 is calculated using equation 4[25, 34, 35]:

$$C_s = \frac{i \times \Delta t}{A \times \Delta V} = \frac{i_A \times \Delta t}{\Delta V} \tag{3}$$

where i_A is the electric current density in $(\frac{A}{cm^2})$, Δt is the discharge time in (s) and ΔV is the potential window in

volts (V). For a current density of 2 $\frac{mA}{cm^2}$ the specific capacitance increased from 29.73 $\frac{mF}{cm^2}$ for the CP to 43.6 $\frac{mF}{cm^2}$ for the CNGO electrodes.

In Fig. 9(a-c), GCD diagram of the CP and CNGO electrodes in currents at current densities of 2, 7, and 15 mA are compared. In all currents current densities, the charging and discharging times of the CNGO electrode have increased compared to CP. Additionally, it is evident that charging and discharging occur more quickly as the current current density increases, due to reduced ion transfer resistance. Higher current density increases the charge passing through the electrode. During charging, higher current density shortens the charging time, reducing energy storage, while during discharging, stored energy is released faster. The longer discharge time leads to higher specific capacitance. The nanocomposite increases surface area, enhances electrochemical reactions, and improves conductivity.

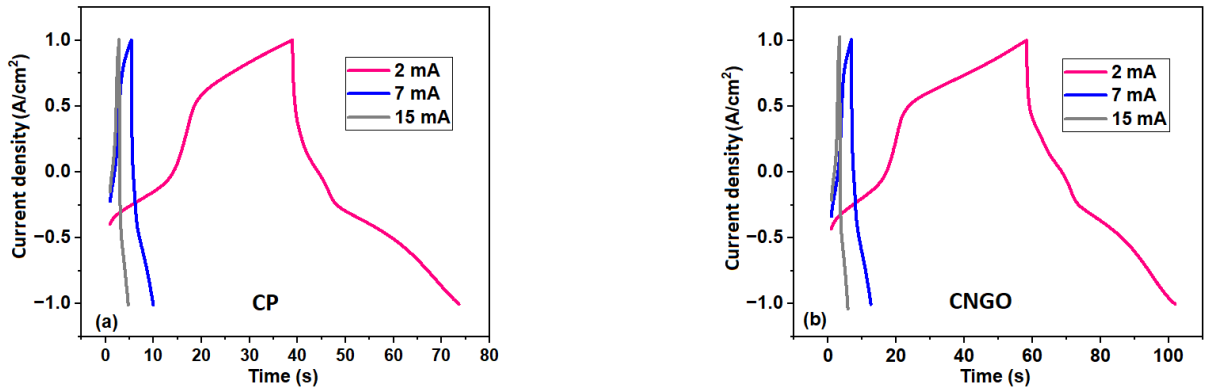

Fig. 8. Galvanostatic charge and discharge diagram of the (a) CP and (b) CNGO electrodes at different current densities

Fig. 10a shows the specific capacitance vs. current density for CP and CNGO electrodes in the current density range from 2 mA/cm² to 15 mA/cm². The presence of the nanocomposite in the CNGO electrode leads to a more porous structure, larger surface area, and higher conductivity, which can increase the accumulation of electrical charge on the electrode.

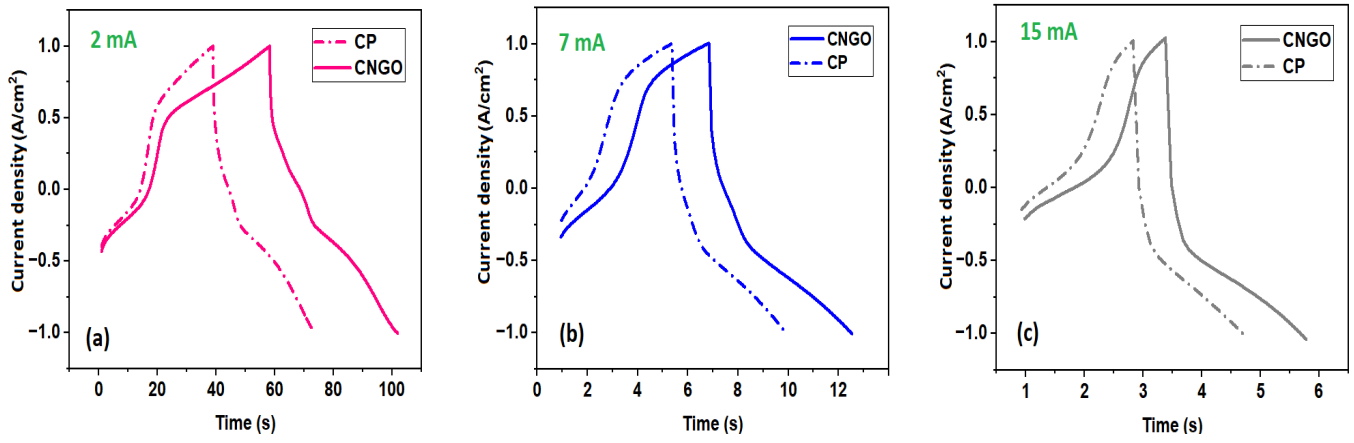

Fig. 9. Galva nostatic charge and discharge diagram of the electrodes in (a) 2 mA, (b)7 mA, and (c) 15 mA

Thus, the increase in electrical conductivity results in an increase in capacitance, energy density, and power density [36]. Fig. 10b shows the energy density versus power density for CP and CNGO electrodes in the range of 2 mA/cm² to 15 mA/cm². Comparing the two electrodes shows that the presence of quasi-capacitive materials in the CP fibers has led to an increase in electrode capacitance, energy density, and power density.

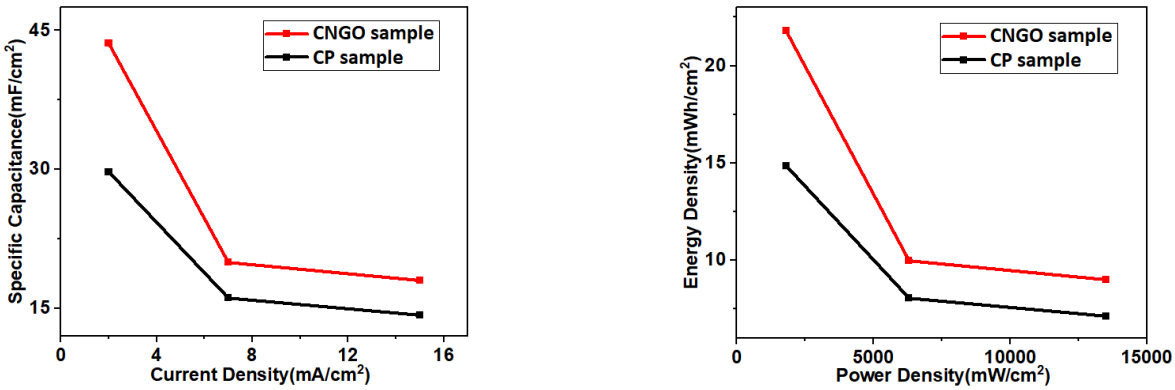

Fig. 10. (a) the specific capacitance versus current density and (b) the energy density versus power density for CP and CNGO electrodes

The Bode plots of electrochemical impedance vs. the logarithm of frequency and phase vs. the logarithm of frequency for CP and CNGO electrodes under open-circuit potential, V_{OCP} (potential under zero current), are shown in Fig. 11a and 11b, respectively. The charge transfer behavior in the electrolyte can be inferred from the electrode-electrolyte resistance in the low-frequency range, but only at the equilibrium position, i.e., the V_{OCP}. At potentials other than V_{OCP}, the electrode-electrolyte characteristics are not reflected in the impedance spectrum due to the complexity of the system conditions. Fig. 11a demonstrates that the electrochemical impedance of the CNGO electrode is lower compared to the CP electrode [37]. The closer the phase angle is to |90°| at low frequencies, the higher the capacitive property of the supercapacitor. At low frequencies, the phase angle (Fig. 11b) of the CNGO electrode is about |−62°|, which is greater than the phase angle of the CP electrode, about |−52.7°|, indicating improved quasi-capacitive properties and better electrode performance. At higher frequencies, the CNGO electrode with a phase angle of |−92.7°| shows a higher capacity than the CP electrode with a phase angle of |−69.5°| [37].

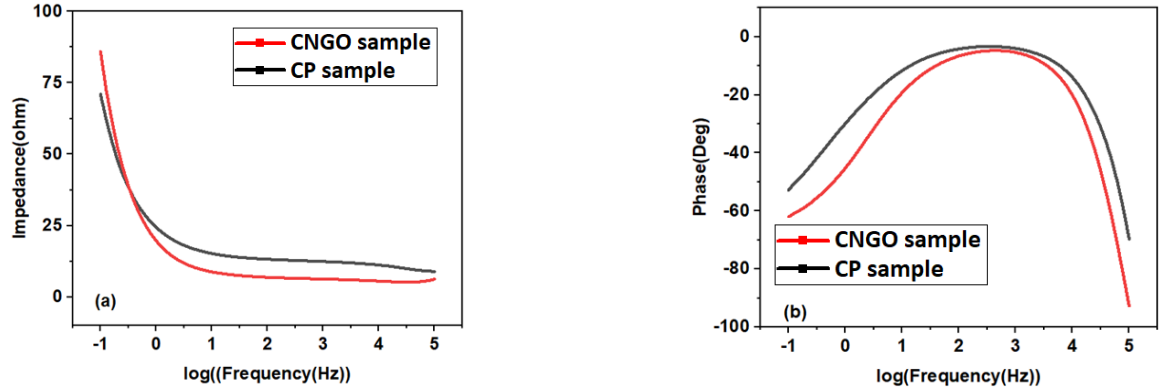

Fig. 11. (a) electrochemical impedance vs. logarithm of frequency and (b) phase diagram vs. logarithm of frequency for CP and CNGO electrodes under open circuit voltage

To evaluate the capacitance retention of the electrode, 1100 cycles were conducted using the GCD method. The sample was repeatedly charged and discharged at room temperature with a current density of 20 mA/cm² to assess the effect of cycling on its capacitance [38, 39]. The results in Fig. 12a indicate that after 1100 cycles, the specific capacitance remains at 100%. In Fig. 12b the potential vs. time for the first charge-discharge cycle is presented. Fig. 12c compares the electrode's response at a current density of 20 mA/cm² during the first three cycles and the last three cycles. The findings demonstrate that the proposed electrode exhibits excellent stability. These attributes make the electrode an excellent candidate for applications requiring long-term stability, high energy efficiency, and sustainable energy storage, such as supercapacitors for green energy technologies.

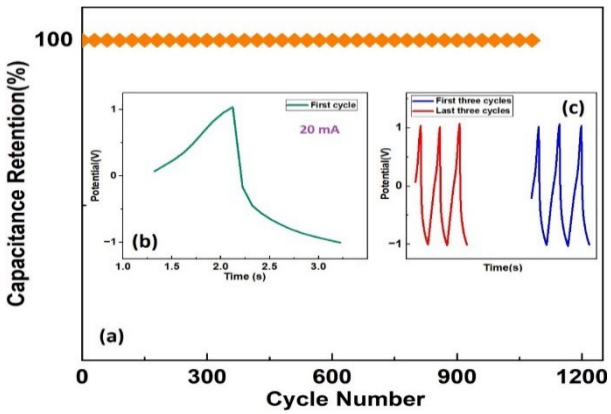

Fig. 12. (a) capacity retention vs. cycle number, (b) potential vs. time for the first charge-discharge cycle, and (c) comparison of the first three charge-discharge cycles with the last three cycles

The provided Nyquist plot (Fig. 13) compares the electrochemical impedance spectra of the CP and CNGO electrodes. The x-axis (Z') represents the real impedance, while the y-axis (-Z'') corresponds to the imaginary impedance. The semicircle's diameter corresponds to the charge transfer resistance at the electrode/electrolyte interface. A smaller diameter means that the electrode material facilitates easier electron transfer and ion movement. In Fig. 13 the semicircle observed in the high-frequency region indicates charge transfer resistance, where the CNGO electrode shows a smaller arc compared to the CP electrode. This suggests that the CNGO electrode has improved charge transfer characteristics, likely due to the enhanced surface area and conductivity introduced by the nanocomposite. At lower frequencies, the steeper curve for the CNGO electrode indicates better capacitive behavior, confirming its potential for use in energy storage applications [40]. The straight line in the Nyquist plot, particularly at the low-frequency region, represents the diffusion behavior of ions within the electrode material, known as the Warburg impedance. A steeper slope indicates better capacitive behavior, suggesting that the electrode material facilitates efficient ion diffusion and storage. The CNGO electrode exhibits a straighter line compared to the CP electrode, implying that the incorporation of the CNGO nanocomposite enhances the diffusion of ions into the electrode structure (Fig. 13). This improvement can be attributed to the increased surface area, porosity, and conductivity provided by the CNGO composite, making it more suitable for energy storage applications such as supercapacitors.

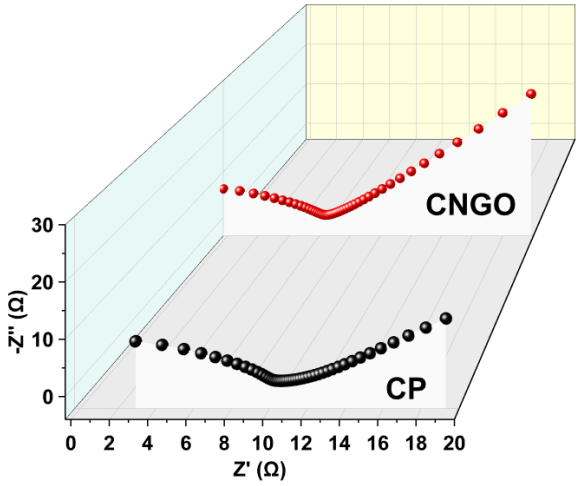

Fig. 13. Nyquist plot of the CP and CNGO electrodes

Table 3 reports the specific capacitance at current densities of 1 and 2 mA/cm² for several supercapacitor electrodes based on carbon materials. The results indicate that the CNGO electrode in sodium phosphate buffer (NaP buffer) electrolyte exhibits higher specific capacitance at a current density of 2 mA/cm². NaP buffer (Na_3PO_4 or Na_2HPO_4/NaH_2PO_4) is commonly employed as an environmentally friendly, non-toxic, and highly conductive electrolyte in supercapacitors and other electrochemical systems. This outcome suggests the optimization of the electrochemical performance of carbon structures in supercapacitors, with a focus on advancing green energy resources.

Table 3. Comparison of the results of this study with the values reported in previous research

	Electrolyte	Current density ($\frac{mA}{cm^2}$)	Specific capacitance ($\frac{mF}{cm^2}$)	Reference
Banana PEEl Carbon	PVA/H_3PO_4	1	33.18	[41]
VACNFs/Diamond	PVA/H_3PO_4	1	30	[42]
VACNFs/Diamond	H_2SO_4 0.1M	2	25	[42]
AC/Cu-BFO	PVA/H_3PO_4	2	15	[43]
CP	NaP Buffer	2	29.73	This work
CNGO	NaP Buffer	2	43.6	This work

4. Conclusion

In this study, a chitosan nitrogen-doped graphene oxide (CNGO) nanocomposite electrode was successfully synthesized and applied to supercapacitor systems. The electrochemical performance of the CNGO electrode was compared to that of CP electrodes, which showed significant improvements. The specific capacitance increased from 29.73 mF/cm² for the CP to 43.6 mF/cm² for the CNGO electrode at a current density of 2 mA/cm². Additionally, the energy density and power density of the CNGO electrode showed substantial enhancement, demonstrating its potential for higher efficiency in energy storage applications. Bode plots and galvanostatic charge-discharge analysis revealed that the CNGO electrode exhibited better stability, faster charge-discharge rates, and improved capacitive behavior. The phase angle data also confirmed superior quasi-capacitive properties at both low and high frequencies, indicating the enhanced electrochemical performance of the CNGO electrode. The reversibility ratio, an important factor for the performance and stability of the electrode, was calculated to be 0.89 for CP and 0.94 for the CNGO electrode, indicating improved charge-discharge reversibility in the CNGO electrode. This higher reversibility ratio, along with increased capacitance and stability, confirms the CNGO nanocomposite's effectiveness in enhancing supercapacitors' performance. The electrode's robust structure ensures minimal degradation during cycling, which is critical for long-term use in energy storage applications. Maintaining 100% capacitance retention showcases its efficiency in storing and releasing energy without significant losses. The choice

of materials, such as nitrogen-doped graphene oxide and chitosan, provides a synergistic combination of high conductivity, a large surface area for ion transport, and enhanced electrochemical activity. These findings highlight the significant improvements in the electrochemical properties of the CNGO electrode, making it a promising candidate for advanced energy storage systems.

References

[1] Muzaffar, A., Ahamed, M.B. and Hussain, C.M., 2024. Green supercapacitors: Latest developments and perspectives in the pursuit of sustainability. *Renewable and Sustainable Energy Reviews*, *195*, p.114324.

[2] Gupta, G.K., Sagar, P., Srivastava, M., Singh, A.K., Singh, J., Srivastava, S.K. and Srivastava, A., 2021. Excellent supercapacitive performance of graphene quantum dots derived from a bio-waste marigold flower (Tagetes erecta). *International Journal of Hydrogen Energy*, *46*(77), pp.38416-38424.

[3] Kumar, Y.A., Roy, N., Ramachandran, T., Hussien, M., Moniruzzaman, M. and Joo, S.W., 2024. Shaping the future of energy: The rise of supercapacitors progress in the last five years. *Journal of Energy Storage*, *98*, p.113040.

[4] Gupta, G.K., Sagar, P., Srivastava, M., Singh, A.K., Singh, J., Srivastava, S.K. and Srivastava, A., 2024. Hydrothermally synthesized nickel ferrite nanoparticles integrated reduced graphene oxide nanosheets as an electrode material for supercapacitors. *Journal of Materials Science: Materials in Electronics*, *35*(3), p.255.

[5] Nawwar, M., Poon, R., Chen, R., Sahu, R.P., Puri, I.K. and Zhitomirsky, I., 2019. High areal capacitance of Fe3O4-decorated carbon nanotubes for supercapacitor electrodes. Carbon Energy, 1(1), pp.124-133.

[6] Polat, S., Mashrah, M. and Maksur, A., 2024. Evaluation of weight, area, and volumetric specific capacitance performance of high graphene content ZnFe2O4 electrode for supercapacitors. *Transactions on Electrical and Electronic Materials*, pp.1-10.

[7] Zhang, W., Shi, J., Webster, R., Li, W. and Li, S., 2024. High-density spherical nanocarbon clusters for pouch-type ionic liquid supercapacitors with high volumetric energy density and rate performance. *Journal of Energy Storage*, *85*, p.111101.

[8] Xue, C.F., Lin, Y., Zhao, W., Wu, T., Wei, Y.Y., Li, X.H., Yan, W.J. and Hao, X.G., 2024. Green preparation of high active biochar with tetra-heteroatom self-doped surface for aqueous electrochemical supercapacitor with boosted energy density. *Journal of Energy Storage*, *90*, p.111872.

[9] Kishore, S.C., Perumal, S., Atchudan, R., Edison, T.N.J.I., Sundramoorthy, A.K., Manoj, D., Alagan, M., Kumar, R.S., Almansour, A.I., Sangaraju, S. and Lee, Y.R., 2024. Sustainable synthesis of spongy-like porous carbon for supercapacitive energy storage systems towards pollution control. *Environmental Science and Pollution Research*, pp.1-12.

[10] Geng, D., Yang, S., Zhang, Y., Yang, J., Liu, J., Li, R., Sham, T.K., Sun, X., Ye, S. and Knights, S., 2011. Nitrogen doping effects on the structure of graphene. Applied Surface Science, 257(21), pp.9193-9198.

[11] Dan, M., Vulcu, A., Porav, S.A., Leostean, C., Borodi, G., Cadar, O. and Berghian-Grosan, C., 2021. Eco-friendly nitrogen-doped graphene preparation and design for the oxygen reduction reaction. Molecules, 26(13), p.3858.

[12] Ali, M.E.A., Aboelfadl, M.M.S., Selim, A.M., Khalil, H.F. and Elkady, G.M., 2018. Chitosan nanoparticles extracted from shrimp shells, application for removal of Fe (II) and Mn (II) from aqueous phases. Separation Science and Technology, 53(18), pp.2870-2881.

[13] Anush, S.M., Chandan, H.R., Gayathri, B.H., Manju, N., Vishalakshi, B. and Kalluraya, B., 2020. Graphene oxide functionalized chitosan-magnetite nanocomposite for removal of Cu (II) and Cr (VI) from waste water. International Journal of Biological Macromolecules, 164, pp.4391-4402.

[14] Clark, G.L. and Smith, A.F., 2002. X-ray Diffraction Studies of Chitin, Chitosan, and Derivatives. The Journal of Physical Chemistry, 40(7), pp.863-879.

[15] Sudhakar, S., Jaiswal, K.K., Peera, S.G. and Ramaswamy, A.P., 2017. Green synthesis of N-graphene by hydrothermal-microwave irradiation for alkaline fuel cell application. Int. J. Recent Sci. Res, 8, pp.19049-19053.

[16] Kumar, M.P., Kesavan, T., Kalita, G., Ragupathy, P., Narayanan, T.N. and Pattanayak, D.K., 2014. On the large capacitance of nitrogen doped graphene derived by a facile route. RSC advances, 4(73), pp.38689-38697.

[17] Khan, A., Goepel, M., Colmenares, J.C. and Gläser, R., 2020. Chitosan-based N-doped carbon materials for electrocatalytic and photocatalytic applications. ACS Sustainable Chemistry & Engineering, 8(12), pp.4708-4727.

[18] Gorgieva, S., Osmić, A., Hribernik, S., Božič, M., Svete, J., Hacker, V., Wolf, S. and Genorio, B., 2021. Efficient chitosan/nitrogen-doped reduced graphene oxide composite membranes for direct alkaline ethanol fuel cells. International journal of molecular sciences, 22(4), p.1740.

[19] Mallakpour, S. and Khadem, E., 2018. Construction of crosslinked chitosan/nitrogen-doped graphene quantum dot nanocomposite for hydroxyapatite biomimetic mineralization. International journal of biological macromolecules, 120, pp.1451-1460.

[20] Kumar, S., Gonen, S., Friedman, A., Elbaz, L. and Nessim, G.D., 2017. Doping and reduction of graphene oxide using chitosan-derived volatile N-heterocyclic compounds for metal-free oxygen reduction reaction. Carbon, 120, pp.419-426.

[21] Fang, Y., Zhang, Q. and Cui, L., 2021. Recent progress of mesoporous materials for high performance supercapacitors. Microporous and Mesoporous Materials, 314, p.110870.

[22] White, R.J. ed., 2015. Porous carbon materials from sustainable precursors. Royal Society of Chemistry.

[23] Pathak, M., Bhatt, D., Bhatt, R.C., Bohra, B.S., Tatrari, G., Rana, S., Arya, M.C. and Sahoo, N.G., 2024. High energy density supercapacitors: an overview of efficient electrode materials, electrolytes, design, and fabrication. The Chemical Record, 24(1), p.e202300236.

[24] Lan, Y. and Changshi, L., 2024. Reliably and accurately estimate energy in super-capacitor via a model of cyclic voltammetry. *Journal of Energy Storage*, *75*, p.109688.

[25] Zhang, S. and Pan, N., 2015. Supercapacitors performance evaluation. Advanced Energy Materials, 5(6), p.1401401.
[26] Sharma, P. and Kumar, V., 2020. Current technology of supercapacitors: A review. Journal of Electronic Materials, 49(6), pp.3520-3532.
[27] Bard, A.J. and Faulkner, L.R., 1983. Electrochemical methods: fundamentals and applications. Surf. Technol, 20(1), pp.91-92.
[28] Elgrishi, N., Rountree, K.J., McCarthy, B.D., Rountree, E.S., Eisenhart, T.T. and Dempsey, J.L., 2018. A practical beginner's guide to cyclic voltammetry. Journal of chemical education, 95(2), pp.197-206.
[29] McCreery, R.L., 2008. Advanced carbon electrode materials for molecular electrochemistry. Chemical reviews, 108(7), pp.2646-2687.
[30] Bard, A.J., Faulkner, L.R. and White, H.S., 2022. Electrochemical methods: fundamentals and applications. John Wiley & Sons.
[31] Rafiee, M., Abrams, D.J., Cardinale, L., Goss, Z., Romero-Arenas, A. and Stahl, S.S., 2024. Cyclic voltammetry and chronoamperometry: mechanistic tools for organic electrosynthesis. *Chemical Society Reviews*.
[32] Jara-Palacios, M.J., Begines, E., Heredia, F.J., Escudero-Gilete, M.L. and Hernanz, D., 2024. Effectiveness of Cyclic Voltammetry in Evaluation of the Synergistic Effect of Phenolic and Amino Acids Compounds on Antioxidant Activity: Optimization of Electrochemical Parameters. *Foods*, *13*(6), p.906.
[33] Pholauyphon, W., Charoen-amornkitt, P., Suzuki, T. and Tsushima, S., 2024. Guidelines for supercapacitor electrochemical analysis: a comprehensive review of methodologies for finding charge storage mechanisms. *Journal of Energy Storage*, *98*, p.112833.
[34] Brett, C.M. and Brett, O., 1993. Principles, methods, and applications. Electrochemistry, 67(2), p.444.
[35] Bard, A.J., Faulkner, L.R. and White, H.S., 2022. Electrochemical methods: fundamentals and applications. John Wiley & Sons.
[36] Zheng, X., Yu, H., Xing, R., Ge, X., Sun, H., Li, R. and Zhang, Q., 2018. Multi-growth site graphene/polyaniline composites with highly enhanced specific capacitance and rate capability for supercapacitor application. *Electrochimica Acta*, *260*, pp.504-513.
[37] Panchal, K., Bhakar, K., Sharma, K.S., Kumar, D. and Prasad, S., 2024. Review on electrochemical impedance spectroscopy: a technique applied to hollow structured materials for supercapacitor and sensing applications. *Applied Spectroscopy Reviews*, pp.1-26.
[38] Reaz, A.H., Saha, S., Roy, C.K., Hosen, M.M., Shuvo, T.S., Islam, M.M. and Firoz, S.H., 2022. Performance improvement of supercapacitor materials with crushed 3D structured graphene. Journal of The Electrochemical Society, 169(1), p.010521.
[39] Ali, G.A., Supriya, S., Chong, K.F., Shaaban, E.R., Algarni, H., Maiyalagan, T. and Hegde, G., 2021. Superior supercapacitance behavior of oxygen self-doped carbon nanospheres: a conversion of Allium cepa peel to energy storage system. Biomass Conversion and Biorefinery, 11, pp.1311-1323.
[40] Wang, G., Zhang, L. and Zhang, J., 2012. A review of electrode materials for electrochemical supercapacitors. Chemical Society Reviews, 41(2), pp.797-828.
[41] Singh, A., Ghosh, K., Kumar, S., Agarwal, A.K., Jassal, M., Goswami, P. and Chaturvedi, H., 2019. Interdigitated flexible supercapacitor using activated carbon synthesized from biomass for wearable energy storage. arXiv preprint arXiv:1903.02384.
[42] Yu, S., Yang, N., Vogel, M., Mandal, S., Williams, O.A., Jiang, S., Schönherr, H., Yang, B. and Jiang, X., 2018. Battery-like supercapacitors from vertically aligned carbon nanofiber coated diamond: design and demonstrator. Advanced Energy Materials, 8(12), p.1702947.
[43] Tanapongpisit, N., Wongprasod, S., Laohana, P., Sonsupap, S., Khajonrit, J., Musikajaroen, S., Wongpratat, U., Yotburut, B., Maensiri, S., Meevasana, W. and Saenrang, W., 2024. Enhancing activated carbon supercapacitor electrodes using sputtered Cu-doped BiFeO3 thin films. Scientific Reports, 14(1), p.27811.